Growth and Physical Properties of $Sr_xCa_{1-x}CrO_3$ Single Crystals

Lipeng Cao [1,2]**, Aizi Jin** [1,3,4]**, Changzhi Gu** [1,3,4]**, Haiyang Bai** [1,3,4]**, Youwen Long** [1,3,4]**, Richeng Yu** [1,3,4]**, Liqing Pan** [2,5,]*** and Changqing Jin** [1,3,4,]*

[1] Institute of Physics, Chinese Academy of Sciences, Beijing 100190, China; clp@iphy.ac.cn (L.C.); azjin@aphy.iphy.ac.cn (A.J.); czgu@iphy.ac.cn (C.G.); hybai@iphy.ac.cn (H.B.); ywlong@iphy.ac.cn (Y.L.); rcyu@iphy.ac.cn (R.Y.)
[2] Department of Physics, University of Science and Technology Beijing, Beijing 100083, China
[3] School of Physics, University of Chinese Academy of Sciences, Beijing 100190, China
[4] Collaborative Innovation Center of Quantum Matter, Beijing 100190, China
[5] College of Science, China Three Gorges University, Yichang 443002, China
* Correspondence: lpan@ctgu.edu.cn (L.P.); jin@iphy.ac.cn (C.J.); Tel.: +86-10-8264-9163 (C.J.)

Abstract: Perovskites $Sr_xCa_{1-x}CrO_3$ attract much attention due to the controversy on the anomalous electronic state. In this study, we synthesized a series of $Sr_xCa_{1-x}CrO_3$ ($0 \leq x \leq 1$) single crystals under high pressure and high temperature conditions with self-oxidization. The crystal structure was determined using X-ray diffraction (XRD). With the increase of x, the structure transformed from orthorhombic to tetragonal to cubic. Antiferromagnetism was observed except for $SrCrO_3$, and the T_N decreased with increased x. All samples demonstrated semiconductive behavior by electrical resistivity measurement.

1. Introduction

Compounds with a perovskite structure are widely researched for their simple crystal structure and abundant emergent phenomena. $ACrO_3$ (A = Ca, Sr, and Pb) were first synthesized at high pressure and high temperature conditions, and their basic physical properties were reported [1–4]. Further research was absent for a long period of time due to difficulties in sample preparation until their anomalous electronic state and associated properties were discovered in recent years [5–7].

The crystal structure of $CaCrO_3$ is orthorhombic with space group Pbnm. The CrO_6 octahedron was compressed along the *c* axis, accompanied by tilt and rotation. $CaCrO_3$ shows C-type antiferromagnetic order with T_N = 90 K [1,8,9]. There exists some controversy on the electrical transport measurement. Polycrystalline samples exhibit insulating behavior, and metallic behavior occurs under high pressure [1,5,10]. However, Weiher et al. claimed that $CaCrO_3$ was metallic through resistivity measurement on a single crystal [11]. Infrared reflectivity measurements on the polycrystalline sample also showed that $CaCrO_3$ was an anomalous antiferromagnetic metallic oxide [12,13]. Theoretical calculations with the local spin-density approximation (LSDA) and LSDA with the on-site Coulomb correlations (U) were undertaken for $CaCrO_3$. Both of these methods provided the correct magnetic ground state, although the magnetic mechanisms were different. However, the former method gives the metallic electronic structure while insulating for the latter one [14,15].

$SrCrO_3$ was considered to be a Pauli paramagnetic metal with cubic crystal structure [2]. Recent research on polycrystalline samples found that a structure phase transition occurred at low temperature accompanied with antiferromagnetism [16,17]. A first-principles calculation based on LSDA suggested that $SrCrO_3$ was a weakly correlated antiferromagnetic metal [18,19]. $SrCrO_3$ is more metallic than $CaCrO_3$ due to its less distorted crystal structure, while a similar controversy about the electronic state also exists. Polycrystalline $SrCrO_3$ shows metallization only under high pressure when the crystal structure remains cubic. Combined with that factor, $SrCrO_3$ becomes more compressible when the pressure is above 4 GPa, when the pressure-induced electronic structure transition to metallic phase occurs [5,20].

A polycrystalline $Sr_xCa_{1-x}CrO_3$ solid solution has been reported previously. The crystal structure transforms from orthorhombic to tetragonal to cubic with the increase of x. The samples are antiferromagnetic except for the cubic phase ones. Insulating behavior was observed for all samples and insulator–metal transition presents under high pressure [10,21–23].
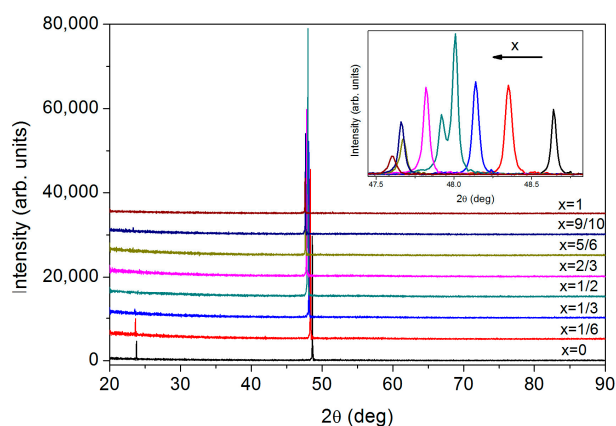
Single crystal samples are essential to investigate the intrinsic properties of these compounds,. There are many challenges in single crystal growth under high pressure, such as the small capsule size, the difficulty in temperature control, and the restriction of control oxygen content since the Cr^{4+} in $(Ca,Sr)CrO_3$ takes an intermediate valence in between the stable one of Cr^{6+} and Cr^{3+}. Therefore, it is difficult to obtain high quality and large single crystals grown under high pressure. In this paper, high quality $Sr_xCa_{1-x}CrO_3$ ($0 \leq x \leq 1$) series single crystals with a size larger than 100 μm are obtained using self-oxidization method, and their basic physical properties are reported.

2. Results and Discussion

2.1. Crystal Growth and Structural Analysis

To obtain $Sr_xCa_{1-x}CrO_3$ single crystals, according to the synthesis conditions reported previously, numerous attempts were made by changing the temperature. It is important to have the correct precursor materials in order to obtain single crystals. The precursor materials for the $Sr_xCa_{1-x}CrO_3$ single crystals growth consist of high purity CrO_2 as well as $Sr(Ca)O$ or $Sr(Ca)O_2$ powders in the appropriate atomic ratio in order to achieve the optimal oxygen pressure at high pressure. This oxygen control process at high pressure is named self-oxidization, since it comes from the composition itself. The advantages of self-oxidization over those using special oxidizers such as $KClO_3$ or $KClO_4$ are: it involves no other elements, so one need not worry about the impurities or unwanted reactions that often happen when using oxidizers; more homogenous sample is available since the composition can be well mixed; it is easy to consistently tune oxygen by changing the atomic ratio in precursor materials [24]. In the case of $CaCrO_3$, it was grown as a bulk sample and the single crystal is shown in Figure 1. In the polycrystalline sample, there were many small embedded cubic-like crystals which could be picked out after the bulk sample was smashed. The optimal temperature was very important: if the temperature was too low, there were no crystals inside, whereas if the temperature was too high, the crystals stuck together and were difficult to isolate. The optimal temperature varied with the content of Sr, so repeated attempts were necessary.

Figure 1. SEM images of (**left**) the bulk sample; and (**right**) the single crystal of $CaCrO_3$.

The crystal structures were first checked by powder XRD. Figure 2 shows the room temperature XRD patterns of $CaCrO_3$. The Rietveld refinement of powder XRD was done using the General Structure Analysis System (GSAS) software package and provided a reliable result. The polycrystalline sample showed a pure phase from which all diffraction peaks could be indexed. The cubic-like single crystal was measured in three directions. The peak position along the c axis slightly shifted to a higher degree due to the compression of the CrO_6 octahedron. The cleavage surface of the single crystal was along the direction of the octahedron connection. The $Sr_xCa_{1-x}CrO_3$ series single crystal XRD patterns are shown in Figure 3. In order to display these patterns more clearly, the $K_{\alpha2}$ peaks were subtracted. The peak position shifted to a lower degree with x, implying that the relative lattice parameter increased with Sr doped. Two adjacent peaks were present in the $Sr_{1/2}Ca_{1/2}CrO_3$ sample. A twin structure possibly formed in the crystal due to the high doping concentration.

(**a**)

(**b**)

Figure 2. The room temperature XRD patterns of $CaCrO_3$ (**a**) powder XRD and Rietveld refinement; (**b**) single crystal XRD of different directions.

Figure 3. The room temperature XRD patterns of $Sr_xCa_{1-x}CrO_3$ single crystals ($K\alpha2$ subtracted).

The room temperature crystal structures of $Sr_xCa_{1-x}CrO_3$ were determined by single-crystal XRD measurement. Table 1 shows the details of structural information. With the increase of x, the crystal structure transformed from orthorhombic to tetragonal to cubic, which was consistent with the previous report [10]; the system became more symmetrical; and there was less distortion in the CrO_6 octahedron. Figure 4 shows the sketch maps of the crystal structures with different space groups.

Table 1. Space groups and structural parameters of $Sr_xCa_{1-x}CrO_3$.

| x	0	1/6	1/3	1/2	2/3	5/6	9/10	1
Space group	Pbnm	Pbnm	I4/mcm	I4/mcm	I4/mcm	Pm3m	Pm3m	Pm3m
a (Å)	5.2702 (11)	5.3081 (9)	5.3484 (16)	5.3627 (3)	5.3785 (4)	3.8141 (1)	3.8096 (1)	3.8146 (1)
b (Å)	5.2933 (10)	5.3144 (7)						
c (Å)	7.4592 (15)	7.5033 (11)	7.567 (3)	7.5655 (11)	7.599 (2)			
<Cr-O-Cr> (deg)	160.01	172.76	180	177.37	180	180	180	180
Primitive cell V (Å³)	52.02 (3)	52.92 (3)	54.12 (5)	54.39 (2)	54.96 (2)	55.49 (1)	55.29 (1)	55.51 (1)
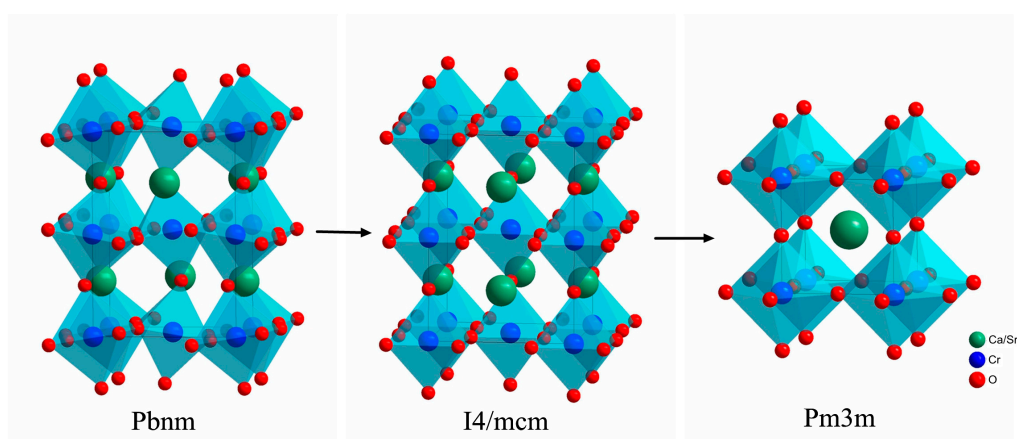
Figure 4. Structural sketch maps of $Sr_xCa_{1-x}CrO_3$ crystals with different space groups.

2.2. Magnetic Properties

The magnetic properties of the single crystals were measured for both the external field parallel and perpendicular to the ab plane. The mass of the crystal was estimated by the volume and structure,

as it is too small to weigh accurately. Only qualitative analyses on the susceptibility measurements were conducted due to the large signal noise and the possible error on mass estimation.

The temperature and field dependence of magnetic moment (MT and MH) curves of $CaCrO_3$ single crystals were measured under different applied field directions, and are shown in Figure 5. Compared with the polycrystalline data reported previously, the single crystal data reveals a very sharp transition at 90 K and obvious magnetic anisotropy. In the case of H parallel to the ab plane, a ferromagnetic-like transition was presented below 90 K and under 1 T external field, with zero-field-cooling (ZFC) and field-cooling (FC) curves completing the overlap. The magnetic hysteresis loop measured at 60 K is also similar to ferromagnetic behavior. Reducing the field to 1000 Oe, the FC curve was slightly depressed, while the ZFC curve dropped dramatically and showed antiferromagnetic behavior. The magnetic moment under one tesla field at low temperature was about 0.017 μ_B per Cr^{4+}, which is a very small value, implying that it was not true ferromagnetism. Considering the previous research showing that $CaCrO_3$ was C-type canted antiferromagnetism [8,9,12], the ferromagnetic behavior should be attributed to the canted spin component, which resulted from the lattice distortion. When H is perpendicular to the ab plane, the MT curves reveal much weaker ferromagnetism and a smaller moment. The MH curves at temperatures below 90 K showed behavior similar to a paramagnetic with weak magnetic order. The magnetic properties of the $SrCrO_3$ single crystal have been published elsewhere. No magnetic transition was observed at low temperature in our sample [25].
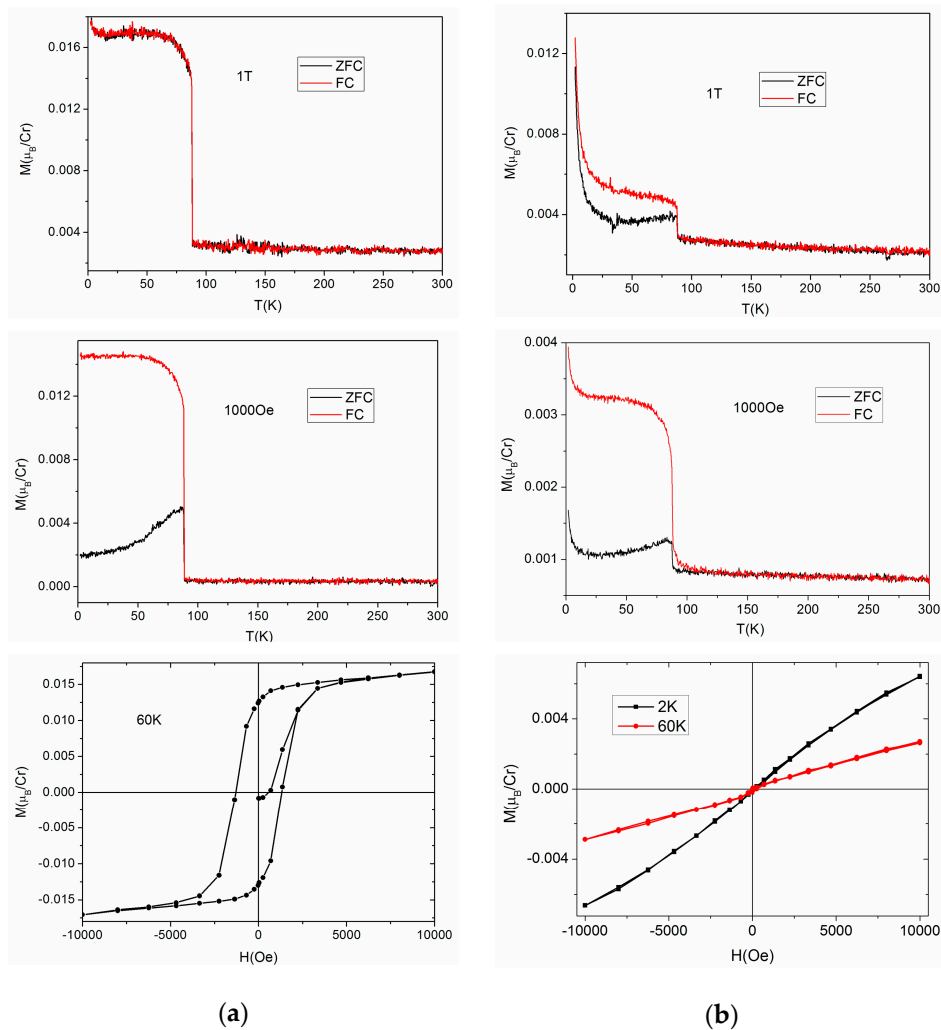

Figure 5. The MT and MH curves of $CaCrO_3$ single crystal with different external field directions (**a**) H//ab plane; (**b**) H ⊥ ab plane. FC: field-cooling; ZFC: zero-field-cooling.

MT curves of samples x = 1/6 and x = 1/3 measured under 1 T external field are shown in Figure 6. The magnetic anisotropy was observed in these two crystals. The ZFC and FC curves were separated below the magnetic transition temperature. The platform in the MT curves was similar to $CaCrO_3$, which was induced by the ferromagnetic component that still exists in $Sr_{1/6}Ca_{5/6}CrO_3$, while it disappeared in $Sr_{1/3}Ca_{2/3}CrO_3$. For the crystals x ≥ 1/2, the MT curves were almost coincident when H along the different edges of the crystal for its less distorted crystal structure. The ZFC and FC curves are overlapped, as shown in Figure 7. The magnetic transition can be observed even at x = 9/10.

Accurate magnetic phase transition temperature T_N can be confirmed from the measurement on single crystal. Figure 8 shows the T_N-composition phase diagram of $Sr_xCa_{1-x}CrO_3$. With the increase of x, T_N decreased gradually from 90 K before finally disappearing. In perovskite ABO_3, the physical properties are closely related to the bond angle B-O-B. The magnetic ordering originates from the superexchange interactions of Cr^{4+}-O-Cr^{4+} in the $Sr_xCa_{1-x}CrO_3$ system. In combination with Table 1, the bond angle of Cr-O-Cr in $CaCrO_3$ was 160°, while it was almost 180° when the structure became tetragonal. When increasing Sr content, the CrO_6 octahedron became less distorted and the Cr-O-Cr bond angle tended to be larger, leading to wider d electronic bandwidth and weaker antiferromagnetic coupling interaction, as well as lower T_N. Meanwhile, the Neel molecular-field theory of antiferromagnetism gave a lower Neel temperature for the sample with a larger primitive cell volume. The T_N of $Sr_xCa_{1-x}CrO_3$ system was influenced by both the Cr-O-Cr bond angle and the cell size [20,26]. As seen in Figure 8, the rate of T_N change with x seems related to the crystal system.

(**a**)   (**b**)
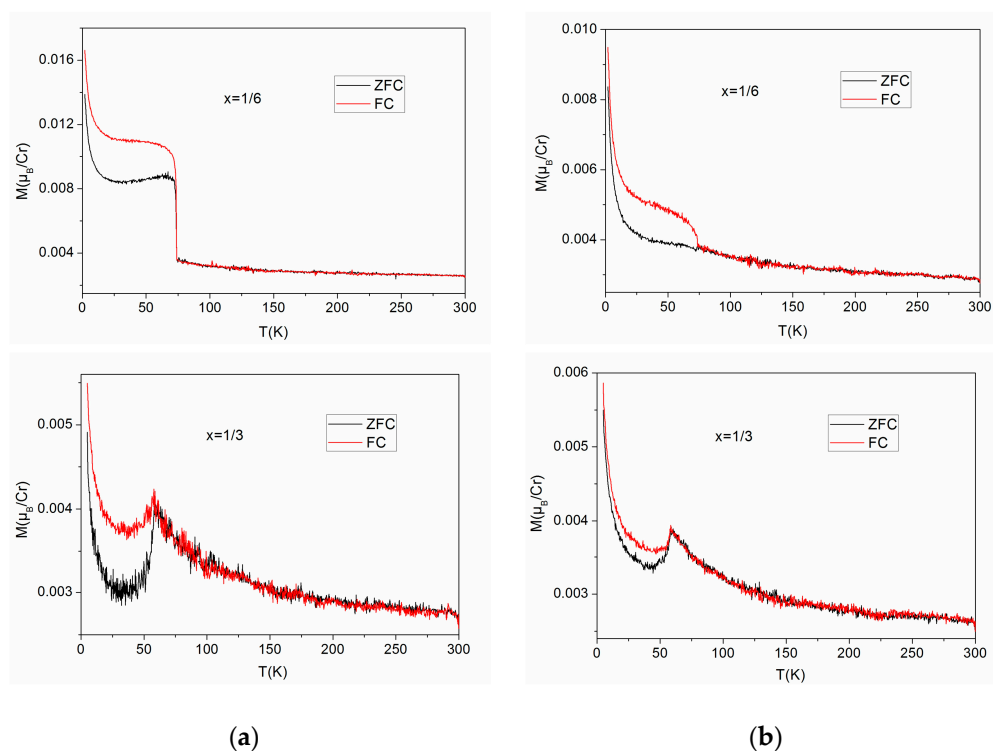
Figure 6. The MT curves of $Sr_{1/6}Ca_{5/6}CrO_3$ and $Sr_{1/3}Ca_{2/3}CrO_3$ single crystals under 1 T external field with different directions (**a**) H//ab plane; (**b**) H ⊥ ab plane.
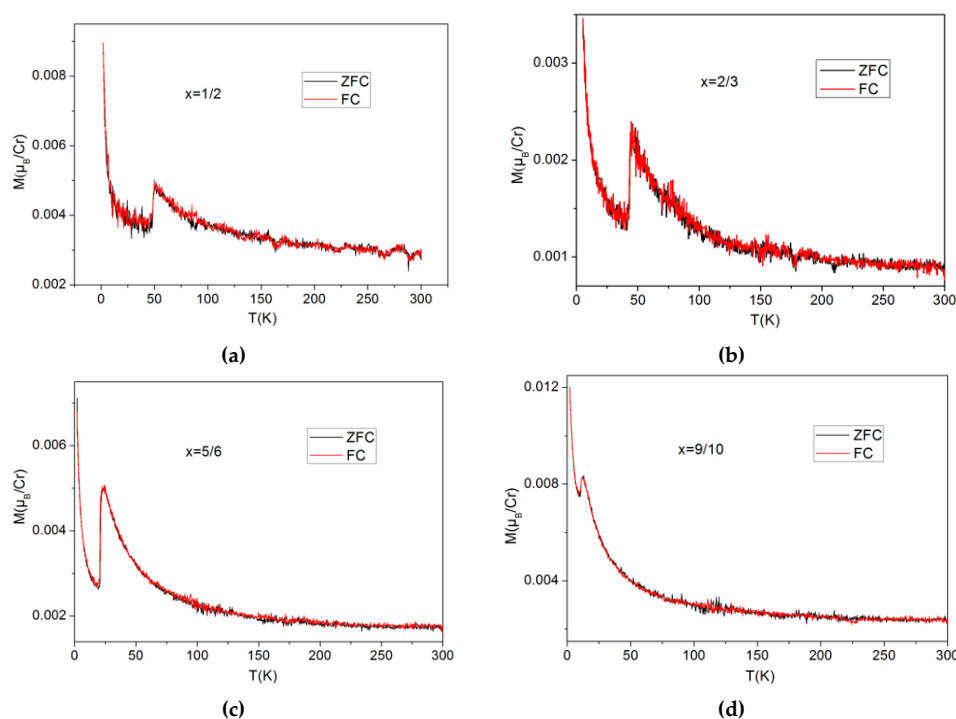
Figure 7. The MT curves under 1 T external field of (**a**) $Sr_{1/2}Ca_{1/2}CrO_3$; (**b**) $Sr_{2/3}Ca_{1/3}CrO_3$; (**c**) $Sr_{5/6}Ca_{1/6}CrO_3$; and (**d**) $Sr_{9/10}Ca_{1/10}CrO_3$ single crystals.
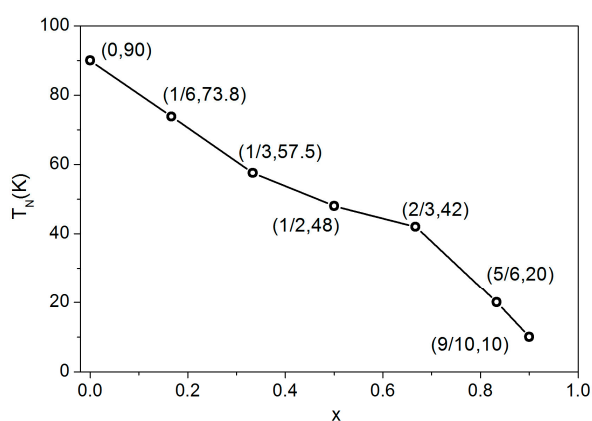

Figure 8. T_N-composition phase diagram of $Sr_xCa_{1-x}CrO_3$.

2.3. Electrical Transport Properties

The electronic state is the focus of controversy in the $Sr_xCa_{1-x}CrO_3$ system. Contrary conclusions were reported from different measurements. In this section, we attempt to prove the electronic state from single crystal resistivity measurements. As the size of single crystals are too small to fabricate electrodes directly, a focused ion beam (FIB) system was used to deposit electrodes on the surface of the single crystal, as shown in Figure 9 with $CaCrO_3$ as an example. The crystal was fixed on the insulating surface of a slice. The bottom edge of the face where the electrodes were deposited required close contact with the sample holder in order to connect the electrodes on the sample and the extraction electrodes on the sample holder. The surface of the sample—especially where electrodes were deposited—was etched using FIB before the deposition of Pt electrodes to avoid the effect of surface pollution and deterioration. The gaps between the electrodes were etched after deposition to clear the possible pollution. Electrical resistivity was estimated, imitating the four-probe method. Considering that the electrodes were limited by the sample shape and deposition rate, and that the contact of electrodes was probably different each time, the current direction was difficult to identify,

therefore leading to errors in quantitative calculations. However, the qualitative characterization should be reliable.
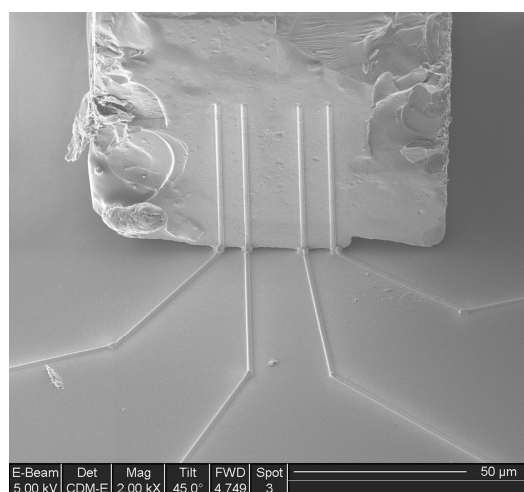
Figure 9. The electrodes deposited by focused ion beam (FIB) system on $CaCrO_3$ single crystal.

The temperature dependence of resistivity measurement results are shown in Figure 10. Although systematic changes with x are not clear, semiconductive behavior was observed for the $Sr_xCa_{1-x}CrO_3$ series samples, implying that localized electronic state in this system was consistent with the polycrystalline measurement result and the recent research on its electronic state [10,27,28]. Without the influence of surface pollution and the grain boundary effect, this result should be more accordant with its intrinsic character.

The semiconductive behavior is inconsistent with the previous result on $CaCrO_3$ reported by Weiher et al. [11]. As mentioned in Reference [11], the single crystal was metal, while there was probably nonstoichiometry in $CaCrO_3$ due to the presence of β-$CaCr_2O_4$, leading to the vacancy of Ca or O. Figure 2 shows that it is a pure phase, even in our bulk $CaCrO_3$ sample. The sample reported here is close to the nominal composition. Zhou et al. [27] measured the specific heat of a single-crystal and polycrystalline $CaCrO_3$. The result indicated that the single-crystal sample with oxygen stoichiometry was insulating while the polycrystalline sample with different oxygen content was metallic [27]. The sample was sensitive to the content of oxygen for its anomalous electronic state, which is located near the localized-itinerant crossover. The contrary conclusion could be attributed to the oxygen vacancy inside, which resulted from different synthesis conditions. Therefore the sample quality is very important to unveil the intrinsic properties of $CaCrO_3$. Here we successfully obtained high quality single crystals using a self-oxidization method that gives rise to more accurately controlled oxygen stoichiometry in the compounds.
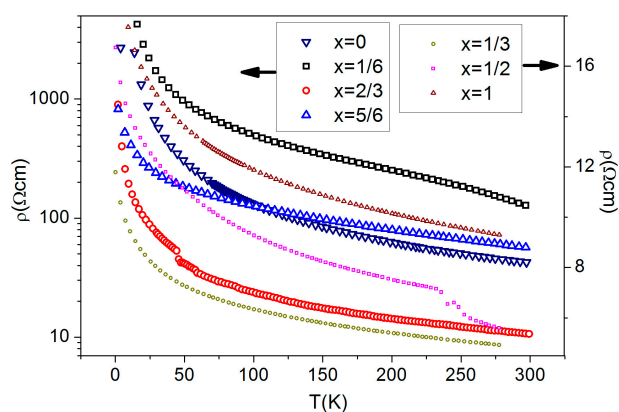
Figure 10. The temperature dependence of resistivity curves of $Sr_xCa_{1-x}CrO_3$ single crystals.

3. Materials and Methods

The sample was assembled using pyrophyllite as a pressure medium and heated by an electric current through a graphite chamber. The temperature was controlled by the heating power. For convenience, the relation curve between power and temperature was measured in advance to provide a reference. The true temperature—which may have errors due to the slight difference of the components used every time—was estimated from the heating power. For the synthesis using self-oxidization method of $Sr_xCa_{1-x}CrO_3$, the pressure was kept at 5.5 GPa and temperature duration was 30 min, with an attempted temperature around 950~1100 °C. In general, the optimal temperatures increased with doping concentration. The bulk sample with embedded single crystals was obtained when the temperature was appropriate.

The bulk samples and crystals were checked using a powder X-ray diffractometer. The Rietveld refinement of the polycrystalline data was undertaken using the GSAS + EXPGUI software package. The diffraction peaks of single crystals were measured for different directions. The sample was placed on a single-crystal silicon wafer, which had no diffraction peaks. Three directions of the cubic-like sample were identified under the microscope. The diffraction peaks were measured under similar conditions for powder and were indexed in contrast to the polycrystalline diffraction data. The structures of the single crystals were determined by single-crystal X-ray diffractometer. The samples were measured at room temperature with Mo Kα radiation. Magnetic properties were performed using the Quantum Design superconducting quantum interference device (SQUID). The three directions of the crystal were measured and the directions were also identified by microscopy. For weak signals of the small crystals, MT curves were measured under the applied field of one tesla. The electrodes were deposited using focused ion beam (FIB) system FEI DB235. FIB is a very powerful tool for in-situ fabrication and characterization of small samples. The surface of the crystal was first etched by a Ga ion beam to clean surface pollution. Next, Pt electrodes and the extraction electrodes were deposited. The thickness of the electrodes was one micron. The largest distance between the extraction electrodes was more than 120 μm. The Pt wires were connected to the extraction electrodes by silver colloid. The electronic resistivity was then measured with the four probe method using the Quantum Design physical property measurement system (PPMS).

4. Conclusions

$Sr_xCa_{1-x}CrO_3$ ($0 \leq x \leq 1$) series single crystals with a size larger than 100 μm were synthesized under high pressure and high temperature condition using self-oxidization method. The crystal structure transformed from orthorhombic to tetragonal to cubic with the increase of x. The crystals showed antiferromagnetic transition at low temperature, with the exception of $SrCrO_3$, and a T_N-composition phase diagram was obtained. Semiconductive behavior was observed for all crystals through electronic resistivity measurements, implying the localized electronic state.

Author Contributions: Changqing Jin conceived and designed the experiments; Lipeng Cao performed the experiments; Lipeng Cao and Changqing Jin analyzed the experimental results; Haiyang Bai provided useful suggestions for measurements; Youwen Long offered helpful proposal for crystal growth; Richeng Yu gave useful discussion on the analysis of crystal structure; Aizi Jin and Changzhi Gu contributed electrodes deposition tools; and Lipeng Cao and Liqing Pan wrote the paper. All authors contributed to the discussions of the paper.

Conflicts of Interest: The authors declare no conflict of interest.

References

1. Goodenough, J.B.; Longo, J.M.; Kafalas, J.A. Band antiferromagnetism and the new perovskite $CaCrO_3$. *Mater. Res. Bull.* **1968**, *3*, 471–481.
2. Chamberland, B.L. Preparation and properties of $SrCrO_3$. *Solid State Commun.* **1967**, *5*, 663–666.
3. Roth, W.L.; Devries, R.C. Crystal and magnetic structure of $PbCrO_3$. *J. Appl. Phys.* **1967**, *38*, 951–952.

4. Devries, R.C.; Roth, W.L. High-pressure synthesis of PbCrO₃. *J. Am. Ceram. Soc.* **1968**, *51*, 72–75.

5. Zhou, J.S.; Jin, C.Q.; Long, Y.W.; Yang, L.X.; Goodenough, J.B. Anomalous electronic state in CaCrO₃ and SrCrO₃. *Phys. Rev. Lett.* **2006**, *96*, 046408.

6. Arevalo-Lopez, A.M.; Alario-Franco, M.A. On the structure and microstructure of "PbCrO₃". *J. Solid State Chem.* **2007**, *180*, 3271–3279.

7. Wu, M.; Zheng, L.R.; Chu, S.Q.; Qin, Z.X.; Chen, X.J.; Lin, C.L.; Tang, Z.; Hu, T.D. Pressure-induced valence change and semiconductor-metal transition in PbCrO₃. *J. Phys. Chem. C* **2014**, *118*, 23274–23278.

8. Alario-Franco, M.A.; Castillo-Martinez, E.; Arevalo-Lopez, A.M. The A(ii)Cr(iv)O₃ (a = Sr, Ca, Pb) 'simple' perovskites. Structure and properties: Magnetic structure of CaCrO₃. *High Press. Res.* **2009**, *29*, 254–260.

9. Ofer, O.; Sugiyama, J.; Mansson, M.; Chow, K.H.; Ansaldo, E.J.; Brewer, J.H.; Isobe, M.; Ueda, Y. Magnetic phase of the perovskite CaCrO₃ studied with μ⁺SR. *Phys. Rev. B.* **2010**, *81*, 184405.

10. Long, Y.W.; Yang, L.X.; Lv, Y.X.; Liu, Q.Q.; Jin, C.Q.; Zhou, J.S.; Goodenough, J.B. Crossover from itinerant-electron to localized-electron behavior in Sr₁₋ₓCaₓCrO₃ perovskite solid solution. *J. Phys. Condens. Matter* **2011**, *23*, 355601.

11. Weiher, J.F.; Chamberland, B.L.; Gillson, J.L. Magnetic and electrical transport properties of CaCrO₃. *J. Solid State Chem.* **1971**, *3*, 529–532.

12. Komarek, A.C.; Streltsov, S.V.; Isobe, M.; Moller, T.; Hoelzel, M.; Senyshyn, A.; Trots, D.; Fernandez-Diaz, M.T.; Hansen, T.; Gotou, H.; et al. CaCrO₃: An anomalous antiferromagnetic metallic oxide. *Phys. Rev. Lett.* **2008**, *101*, 167204.

13. Komarek, A.C.; Moller, T.; Isobe, M.; Drees, Y.; Ulbrich, H.; Azuma, M.; Fernandez-Diaz, M.T.; Senyshyn, A.; Hoelzel, M.; Andre, G.; et al. Magnetic order, transport and infrared optical properties in the ACrO₃ system (a = Ca, Sr, and Pb). *Phys. Rev. B* **2011**, *84*, 125114.

14. Streltsov, S.V.; Korotin, M.A.; Anisimov, V.I.; Khomskii, D.I. Band versus localized electron magnetism in CaCrO₃. *Phys. Rev. B* **2008**, *78*, 054425.

15. Liu, H.M.; Zhu, C.; Ma, C.Y.; Dong, S.; Liu, J.M. Fragile magnetic ground state and metal-insulator transitions in CaCrO₃: The first-principles calculations. *J. Appl. Phys.* **2011**, *110*, 073701.

16. Williams, A.J.; Gillies, A.; Attfield, J.P.; Heymann, G.; Huppertz, H.; Martinez-Lope, M.J.; Alonso, J.A. Charge transfer and antiferromagnetic insulator phase in SrRu₁₋ₓCrₓO₃ perovskites: Solid solutions between two itinerant electron oxides. *Phys. Rev. B* **2006**, *73*, 104409.

17. Ortega-San-Martin, L.; Williams, A.J.; Rodgers, J.; Attfield, J.P.; Heymann, G.; Huppertz, H. Microstrain sensitivity of orbital and electronic phase separation in SrCrO₃. *Phys. Rev. Lett.* **2007**, *99*, 255701.

18. Lee, K.W.; Pickett, W.E. Orbital-ordering driven structural distortion in metallic SrCrO₃. *Phys. Rev. B* **2009**, *80*, 125133.

19. Qian, Y.M.; Wang, G.T.; Li, Z.; Jin, C.Q.; Fang, Z. The electronic structure of a weakly correlated antiferromagnetic metal, SrCrO₃: First-principles calculations. *New J. Phys.* **2011**, *13*, 053002.

20. Jin, C.Q.; Liu, Q.Q.; Long, Y.W.; Zhao, J.G.; Lu, Y.X.; Yang, L.X.; Zhu, J.L.; Wang, X.C. High-pressure synthesis and properties of new functional compounds. *Phys. Status Solidi A* **2010**, *207*, 2750–2756.

21. Yang, L.X.; Long, Y.W.; Jin, C.Q.; Yu, R.C.; Zhou, J.S.; Goodenough, J.B.; Liu, H.Z.; Shen, G.Y.; Mao, H.K. Pressure induced metallization in ACrO₃ in perovskite compounds. *J. Phys. Conf. Ser.* **2008**, *121*, 022017.

22. Castillo-Martinez, E.; Duran, A.; Alario-Franco, M.A. Structure, microstructure and magnetic properties of Sr₁₋ₓCaₓCrO₃ (0 ≤ x ≤ 1). *J. Solid State Chem.* **2008**, *181*, 895–904.

23. Castillo-Martinez, E.; Arevalo-Lopez, A.M.; Ruiz-Bustos, R.; Alario-Franco, M.A. Increasing the structural complexity of chromium(iv) oxides by high-pressure and high-temperature reactions of CrO₂. *Inorg. Chem.* **2008**, *47*, 8526–8542.

24. Jin, C.Q. High pressure synthesis of novel high Tᶜ superconductors. *High Press. Res.* **2004**, *24*, 399–408.

25. Cao, L.P.; Pan, L.Q.; Li, W.M.; Wang, X.C.; Liu, Q.Q.; Long, Y.W.; Gu, C.Z.; Jin, C.Q. High pressure growth and characterization of SrCrO₃ single crystal. *Int. J. Mod. Phys. B* **2015**, *29*, 1542025.

26. Goodenough, J.B. Localized versus collective d electrons and neel temperatures in perovskite and perovskite-related structures. *Phys. Rev.* **1967**, *164*, 785–789.

27. Zhou, J.S.; Alonso, J.A.; Sanchez-Benitez, J.; Fernandez-Diaz, M.T.; Martinez-Coronado, R.; Cao, L.P.; Li, X.; Marshall, L.G.; Jin, C.Q.; Goodenough, J.B. Identification of electronic state in perovskite CaCrO₃ by high-pressure studies. *Phys. Rev. B* **2015**, *92*, 144421.

28. Zhou, J.S.; Cao, L.P.; Alonso, J.A.; Sanchez-Benitez, J.; Fernandez-Diaz, M.T.; Li, X.; Cheng, J.G.; Marshall, L.G.; Jin, C.Q.; Goodenough, J.B. Possible bose-einstein condensate associated with an orbital degree of freedom in the mott insulator $CaCrO_3$. *Phys. Rev. B* **2016**, *94*, doi:10.1103/PhysRevB.94.155137.